# Investigating the Role of Solvent–Solute Interaction in Crystal Nucleation of Salicylic Acid from Organic Solvents

**ARTICLE** *in* JOURNAL OF THE AMERICAN CHEMICAL SOCIETY · JULY 2014

Impact Factor: 12.11 · DOI: 10.1021/ja503131w · Source: PubMed



**4 AUTHORS**, INCLUDING:

Dikshitkumar Khamar
University of Limerick
**9** PUBLICATIONS **79** CITATIONS
SEE PROFILE

Jacek Zeglinski
University of Limerick
**15** PUBLICATIONS **85** CITATIONS
SEE PROFILE

Åke C. Rasmuson
University of Limerick
**122** PUBLICATIONS **1,774** CITATIONS
SEE PROFILE

JACS
JOURNAL OF THE AMERICAN CHEMICAL SOCIETY

Article

pubs.acs.org/JACS

# Investigating the Role of Solvent–Solute Interaction in Crystal Nucleation of Salicylic Acid from Organic Solvents

Dikshitkumar Khamar,[†] Jacek Zeglinski,[†] Donal Mealey,[†] and Åke C. Rasmuson*[,†,‡]

[†]Materials and Surface Science Institute, Department of Chemical and Environmental Science, University of Limerick, Limerick, Ireland

[‡]Department of Chemical Engineering and Technology, KTH Royal Institute of Technology, SE-100 44 Stockholm, Sweden

Supporting Information

**ABSTRACT:** In previous work, it has been shown that the crystal nucleation of salicylic acid (SA) in different solvents becomes increasingly more difficult in the order: chloroform, ethyl acetate acetonitrile, acetone, methanol, and acetic acid. In the present work, vibration spectroscopy, calorimetric measurements, and density functional theory (DFT) calculations are used to reveal the underlying molecular mechanisms. Raman and infrared spectra suggest that SA exists predominately as dimers in chloroform, but in the other five solvents there is no clear evidence of dimerization. In all solvents, the shift in the SA carbonyl peak reflecting the strength in the solvent–solute interaction is quite well correlated to the nucleation ranking. This shift is corroborated by DFT calculated energies of binding one solvent molecule to the carboxyl group of SA. An even better correlation of the influence of the solvent on the nucleation is provided by DFT calculated energy of binding the complete first solvation shell to the SA molecule. These solvation shell binding energies are corroborated by the enthalpy of solvent–solute interaction as estimated from experimentally determined enthalpy of solution and calculated enthalpy of cavity formation using the scaled particle theory. The different methods reveal a consistent picture and suggest that the stronger the solvent binds to the SA molecule in solution, the slower the nucleation becomes.

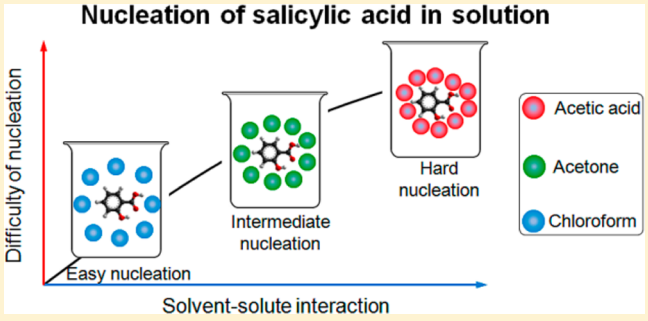


## INTRODUCTION AND BACKGROUND

Crystal nucleation from solution is one of the classical not well understood phenomena of chemistry—perhaps deserving to be called a "grand challenge". Crystal nucleation is a widely occurring phenomenon in nature, e.g., in the formation of bones, shells, and ice, is of significant industrial importance in the manufacturing of many inorganic and organic materials, and has medical implications, e.g., in the formation of kidney stones and precipitates of amyloid proteins. Crystal nucleation is a key step in crystallization of pharmaceutical compounds and has a governing influence on the product crystal size distribution and polymorphic outcome. Unfortunately, the fundamental understanding of crystal nucleation from solution is still insufficient, and crystallization processes have to be developed based on scaling-up of laboratory experiments. As an alternative to the classical nucleation theory the two-step mechanism has been recently proposed,[1−3] but the nucleation behavior of a new compound is far from being predictable from first-principles, and experimental results are sensitive to the detailed design of the experiments.

The solvent often has a significant influence on the nucleation behavior of a substance, and experiments with different solvents can be used to probe the mechanisms of nucleation. Within the classical nucleation theory the influence of the solvent is primarily explained in terms of the solid–liquid interfacial energy.[4,5] However, other studies have also considered the pre-exponential factor.[6] A common approach is to analyze from the point of view of molecular structuring in solution.[2,7] It is suggested that the competition between different hydrogen-bonded (H-bonded) aggregates in reaching the critical nucleus size determines the solid phase that will appear, and that solvent influences the formation of these H-bonded aggregates.[8−11] Janik et al.[8] could explain differences in the formation of different polymorphs based on differences in solvation. By comparing infrared (FTIR) spectra of benzoic and tetrolic acid solutions with that of the solid phases, Davey et al.[12] were able to find a link between solution structuring and the crystallizing solid phase, but in the case of mandelic acid this link could not be established. Modeling approaches are increasingly finding place in understanding nucleation phenomenon,[13−15] adopting quantum mechanical description or molecular mechanics as well as molecular dynamics.

In a previous paper[16] a detailed experimental study over the crystal nucleation of salicylic acid (SA) in a range of different solvents is reported. Experimental induction time distributions reveal that in order to achieve the same induction time the lowest driving force is required in chloroform followed in order

**Received:** March 28, 2014
**Published:** July 16, 2014

   dx.doi.org/10.1021/ja503131w | J. Am. Chem. Soc. 2014, 136, 11664−11673

of increasing driving force by ethyl acetate, acetonitrile, acetone, methanol, and acetic acid (AA). By evaluation in accordance with the classical nucleation theory, the interfacial energy is found to increase in the same order: chloroform (0.71 mJ $m^{-2}$), ethyl acetate (1.82 mJ $m^{-2}$), acetonitrile (2.40 mJ $m^{-2}$), acetone (3.81 mJ $m^{-2}$), methanol (4.13 mJ $m^{-2}$), and AA (5.50 mJ $m^{-2}$). In the present work, we undertake (i) Raman and infrared spectroscopic investigations, (ii) calorimetric measurements of the enthalpy of solution and, and (iii) molecular modeling in order to investigate solvent−solute interactions in solution and solute dimerization. These results are then used to explain the nucleation behavior.

SA is a simple essentially nonflexible molecule, for which only one crystal structure is known. This facilitates the interpretation of experimental data and the analysis of possible mechanisms. The crystal structure is based on centrosymmetric dimerization over the carboxyl groups, Figure 1.

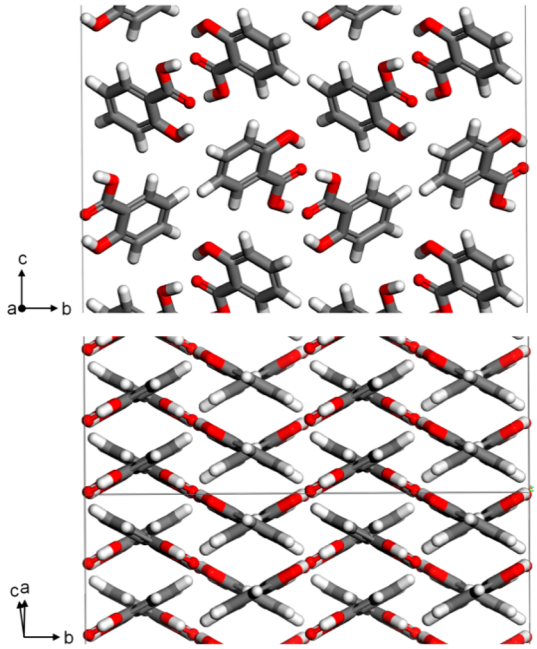


**Figure 1.** Molecular arrangement in crystal lattice of SA. View along crystallographic *a*-axis and array of stacked SA dimers.

## EXPERIMENTAL AND COMPUTATIONAL METHODS

SA with ≥99% purity was purchased from Sigma-Aldrich and used as received. Analytical grade solvents (methanol, acetone, acetonitrile, ethyl acetate, chloroform, and glacial AA), purchased from VWR International, with ≥99.7% purity were used without any further treatment.

**Vibrational Spectroscopy.** In situ IR and Raman spectroscopy has been used to investigate the molecular structuring in solutions of SA at various concentrations in the six solvents. Solution spectra are compared with those of the pure SA solid and melt. For Raman spectroscopy, a Kaiser Raman Rxn2 analyzer with an Invictus 785 nm excitation laser and CCD camera (DV420-OE) based detector was used. A short focus, immersion probe of 1/4 in. diameter was used for the liquid samples, and a noncontact probe was employed for the solid samples. Each spectrum was collected for a minimum of 10 s exposure time and three accumulations in the spectral region of 3400−200 $cm^{-1}$. Data collection and the solvent subtraction were carried out using Mettler Toledo iC Raman software version 4.1.

IR spectra of the solid form were collected using a PerkinElmer, spectrum 100 spectrometer fitted with universal ATR accessory (single reflection and diamond/zinc selenide material) and lithium tantalate detector. In total, 56 scans were collected per spectrum with resolution of 4 $cm^{-1}$ in the spectral region of 4000−400 $cm^{-1}$. Solution spectra were collected using Mettler Toledo ReactIR 10 fitted with a silver halide probe composed of diamond composite and mercury cadmium telluride (MCT) detector cooled with liquid nitrogen. For each spectrum, 167 scans were collected from 2000 to 650 $cm^{-1}$ at 4 $cm^{-1}$ resolution using iC IR software version 4.3. All the spectral data were collected at ambient temperature (20−22 °C), unless mentioned otherwise. Due to the strong absorption of the solvent carbonyl group, IR spectra in acetone, ethyl acetate, and AA solutions have not been collected.

For collection of Raman and IR spectra from the melt, the probe was inserted into a glass vial containing crystalline material before sealing it with a tight cap. The vial was kept inside a copper block to give uniform heating and to minimize sublimation during heat cool cycles. The spectra were collected at 90 °C as the supercooled melt crystallized at temperature lower than that.

**Solution Calorimetry.** Solution calorimetry has been used to determine the enthalpy of solution of SA in the six different solvents, and from that the enthalpy of solute−solvent interaction was calculated. A semiadiabatic type, Precision Solution Calorimeter (TA Instruments, USA) was used together with the Thermal Activity Monitor, TAM III giving a temperature control of 0.0001 °C. In each experiment, 325−330 mg of SA was dissolved in 100 mL solvent. The variation among multiple runs was <0.21 kJ $mol^{-1}$. A novel, PTFE tape based sealing technique was used to cap the ampule since the normal silicone bung and bee wax method is not compatible with the organic solvents used. First, a small quantity of PTFE tape was firmly attached on the ampule hole. On that, the silicone rubber bung was fixed, and finally tape was tightly rolled over twice. In this way only PTFE and glass was in contact with solid and solvent. The calibration was checked against dissolution of KCl in deionized water and was 0.05 kJ $mol^{-1}$ different from the calibration without PTFE tape.

From the experimentally determined enthalpy of solution, $\Delta H_{solution}$, the enthalpy of solvation, $\Delta H_{solvation}$, can be calculated if the enthalpy of sublimation, $\Delta H_{sublimation}$, is known:

$$\Delta H_{solvation} = \Delta H_{solution} - \Delta H_{sublimation} \quad (1)$$

and represents the enthalpy change upon transferring a solute molecule from the vapor phase into the solution. The value for $\Delta H_{sublimation}$ for SA at 25 °C has been reported to be 94.4 kJ $mol^{-1}$.[17] The enthalpy of solvation includes breaking solvent−solvent bonds and forming solvent−solute bonds and is given by eq 2:[18,19]

$$\Delta H_{solvation} = \Delta H_{cavity} + \Delta H_{interaction} + \alpha RT^2 - RT \quad (2)$$

where, $\Delta H_{cavity}$ includes endothermic contributions related to the formation of a cavity in the solvent to incorporate the solute molecule, $\Delta H_{interaction}$ is the enthalpy of solvent−solute bonding, and $\alpha$ is the isobaric thermal expansion coefficient of the solvent. In addition to cavity and interaction terms, enthalpy of solvation can also include endothermic contributions from the conformational changes of flexible molecules.[19,20] However, since SA is a small and rigid molecule, such terms have been neglected.

The enthalpy of cavity formation, $\Delta H_{cavity}$, is calculated by the scaled particle theory (SPT), developed by Reiss[21] and later revised by Pierotti[22] as[22,23]

$$\Delta H_{cavity} = \alpha RT^2 \frac{y}{(1-y)^3}\left\{(1-y)^2 + 3(1-y)\left(\frac{D_2}{D_1}\right) + 3(1+2y)\left(\frac{D_2}{D_1}\right)^2\right\} + PV_1 y\left(\frac{D_2}{D_1}\right)^3 \quad (3)$$

where the enthalpy is obtained per mole of solute, $y = N_A \pi {D_1}^3/6V_1$; $V_1$ is molar volume; $D_1$ and $D_2$ are solvent and solute molecular diameter, respectively, $P$ is pressure, $N_A$ is the Avogadro's number, $R$ is the gas


dx.doi.org/10.1021/ja503131w | J. Am. Chem. Soc. 2014, 136, 11664−11673

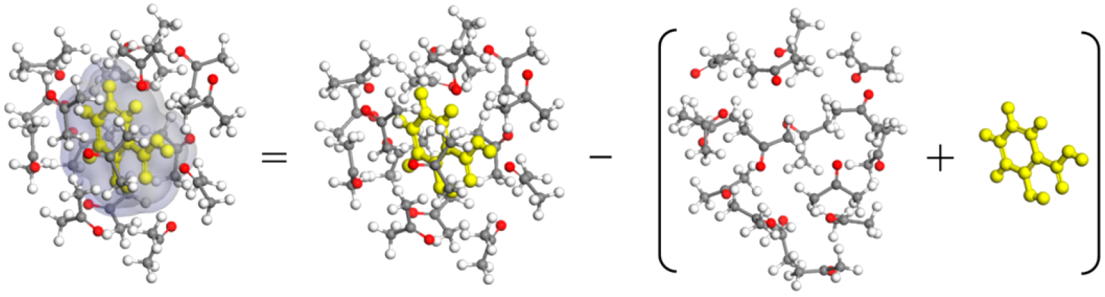

**Figure 2.** A method for quantifying binding energy ($\Delta E_{solvation}$) in a solvation cluster between a solute molecule (yellow) and a shell of solvent molecules.

constant, and $T$ the temperature (K). A detailed discussion about the SPT,[21,22] its application,[19,23−25] and limitations[26,27] can be found in the literature. In the present work molecular diameters were calculated using Bondi's van der Waal radii in the Material Studio software. The values of molecular diameters, isobaric thermal expansion coefficients, and other constants used to calculate the cavity term are given in the Supporting Information file. Knowing the enthalpy of cavity formation, $\Delta H_{cavity}$, the enthalpy of interaction, $\Delta H_{interaction}$, can be calculated from eq 2.

**Quantum Chemical Calculations.** Density functional theory (DFT) calculations have been applied using a Gaussian 09 package[28] to investigate interactions in (1:1) molecular complexes of SA in the six solvents. The solvent−solute interactions are probed at both polar and nonpolar sites of the SA molecule. In addition, the first solvation shell of the SA molecule is modeled in all six solvents, based on the insights about geometry and energetics in the different solvents derived from the (1:1) molecular models. In building the solvation cluster models, at first, four solvent molecules are placed around a "core" molecule of SA at a distance and location found for the optimized (1:1) complexes. Subsequent solvent molecules are placed between these four molecules. Due to different molecular sizes and intermolecular distances specific to each solvent, the solvation shells are composed of different number of solvent molecules to allow for a uniform coverage of the space around the SA molecule. Number of atoms/nm$^3$ in a solvation shell is calculated from Connolly surfaces generated in the Materials Studio software (ver. 4.4).

The equilibrium geometries of the modeled associates are calculated with a B97D Grimme's functional,[29] which includes a long-range dispersion correction. This allows for better description of the van der Waals interactions and gives proper geometries of molecular clusters.[30] Binding energies of the complexes are calculated using a double hybrid B2PLYPD functional,[31] which combines exact Hartree−Fock exchange with an MP2-like correlation and long-range dispersion corrections. A Gaussian-type 6-31G(d,p) basis set[32] is used for geometry optimization and a triple-$\zeta$ valence quality (TZVP) basis set[33] is used for energy calculations of the (1:1) associates. Basis set superposition error (BSSE) is calculated for these systems to correct overestimation in binding energies due to the overlapping of basis functions.[34] The BSSE corrected binding energies include monomer deformation as calculated according to eq 1S (Supporting Information file).

The uncorrected binding energy between two molecules (three in case of transition-state modeling discussed below) is calculated as follows:

$$\Delta E_{bind} = E_{A\text{-}B\ldots\text{-}N} - (E_A + E_B + \ldots + E_N) \quad (4)$$

where $E_{A\text{-}B\ldots\text{-}N}$ is the energy of a molecular cluster (dimer, trimer etc.) and $E_A$, $E_B$, and $E_N$ are the energies of isolated monomers A, B, ..., and N in fully relaxed gas phase geometries. The binding energy of the solvation cluster quantifies the cohesive strength of the entire cluster of one SA molecule surrounded by the first solvation shell of solvent molecules and is calculated as

$$\Delta E_{bind} = E_{solvation\text{-}cluster} - (nE_{solvent} + E_{solute}) \quad (5)$$

where $E_{solvation\text{-}cluster}$ is the energy of the solvent-SA cluster containing $n$ molecules of a solvent. $E_{solvent}$ and $E_{solute}$ are the energies of the solvent and the solute, respectively, in their fully relaxed gas-phase geometries. The binding energy in the solvation cluster between a solute molecule and the surrounding solvation shell has been defined here as the electronic solvation energy, $\Delta E_{solvation}$, and calculated as is illustrated schematically in Figure 2, using eq 6:

$$\Delta E_{solvation} = E_{solvation\text{-}cluster} - (E_{solvent\text{-}shell} + E_{solute}^{constrained}) \quad (6)$$

where $E_{solvation\text{-}cluster}$ is a single point energy of the optimized solvation cluster, $E_{solvent\text{-}shell}$ is a single point energy calculated for the solvent-shell structure after removal of the solute molecule from the solvation cluster, however retaining the position and geometry of the solvent molecules as if the solute molecule is still in the center. $E_{solute}^{constrained}$ is a single point energy calculated for that removed solute (SA) molecule being in its constrained solvation-cluster geometry. To the best of our knowledge the presented method of quantifying solvent shell−solute core interactions in a first solvation shell cluster (eq 6, Figure 2) has not been reported before. Considering the complexity of the solvation cluster models, we have not corrected these systems for BSSE. Instead, we have used a larger basis set of quadruple-$\zeta$ valence quality (QZVP) to calculate binding energies;[35] a well-known strategy to reduce BSSE.[30]

The energy associated with the deformation of the SA molecule within the solvation shell, the deformation energy, $\Delta E_{deform}$, was calculated as the difference in energy of the solvation shell constrained geometry of the solute molecule, $E_{solute}^{constrained}$, and the fully relaxed gas-phase geometry of the SA molecule.

## RESULTS

**Spectroscopic Investigations.** *Solid and Melt Spectra.* The IR and Raman spectra of solid crystalline material of SA (Figure 3) show strong bands for the carbonyl stretching at 1655 and 1637 cm$^{-1}$, respectively. From the crystal structure of SA (Figure 1) it is clear that this carbonyl stretching corresponds to a carbonyl group involved in the centrosymmetric dimerization. In comparison to benzoic acid IR,[12] the carbonyl absorption frequency for SA is lower because the carbonyl group is also influenced by the intramolecular hydrogen bonding to the alcohol group in the ortho position. This could also be the reason why the out of plane bending of the O−H group that is characteristic to carboxylic acid dimers[36] appears differently in case of SA. In benzoic acid, *m*-hydroxy benzoic acid and *p*-hydroxy benzoic acid the carboxylic acid dimer motif give rise to a broad, out of plane bending peak centered around 930 cm$^{-1}$. For the SA dimer, there is no clear peak in this region. Instead, there is a weak peak at 965 cm$^{-1}$ and a broad peak at 888 cm$^{-1}$ with a shoulder peak at 915 cm$^{-1}$. Detailed spectra of these four acids are shown in the Supporting Information file. The Raman spectra of the SA melt in Figure 3 show two peaks in the carbonyl region; a strong peak at 1641 and a weak peak at 1692 cm$^{-1}$. This suggests that


dx.doi.org/10.1021/ja503131w | J. Am. Chem. Soc. 2014, 136, 11664−11673

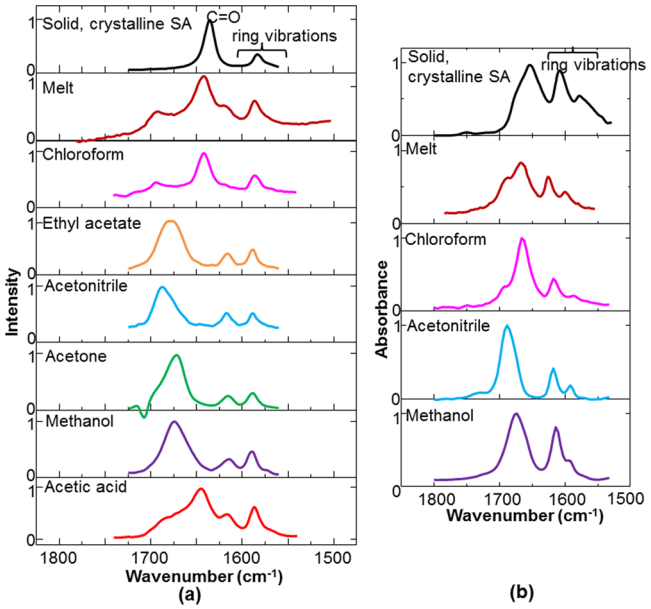


**Figure 3.** (a) Raman spectra of crystalline SA in comparison with spectra of melt and SA solutions. (b) IR spectra of crystalline SA in comparison with spectra of melt and SA solutions. Solvent spectrum is subtracted from the solution spectra. The spectra in methanol, acetone, and ethyl acetate solutions are collected for 100–120 g/kg, solution in acetonitrile at 79 g/kg, and solution in chloroform at 10 g/kg concentration.

in the melt, the dimer motif of SA is essentially preserved, with some appearance of more loosely bound/monomer molecules of SA evidenced by the small peak at higher wavenumber. IR data complements the Raman spectra.

*Solution Spectra.* The Raman spectra in chloroform (Figure 3a) shows a very slight carbonyl shift only compared to the solid (from 1637 $cm^{-1}$ in solid SA to 1642 $cm^{-1}$ in chloroform solutions) suggesting significant dimerization of SA molecules. Apart from the strong peak at 1642 $cm^{-1}$, there is also a low intensity peak at 1692 $cm^{-1}$, indicating that a smaller fraction of the SA molecules are present as monomers. The IR spectra of SA in chloroform (Figure 3b) show similar results; a strong carbonyl peak corresponding to SA dimerization is found at 1664 $cm^{-1}$, and a small shoulder corresponding to monomer of SA is seen at 1692 $cm^{-1}$.

Raman spectra for SA in the four solvents: ethyl acetate, acetonitrile, acetone, and methanol show a larger shift of the dominating carbonyl peak to higher wavenumbers (Figure 3a). Compared to chloroform, the dominating carbonyl peak in acetone and methanol appears at wavenumbers 36–40 $cm^{-1}$ higher, Table 1. In the ethyl acetate solution the carbonyl peak is shifted by 42 $cm^{-1}$ and in acetonitrile by 50 $cm^{-1}$. This shift suggests that in these solvents SA is present predominantly as monomer, and there is no or only a weak indication of dimer formation. Methanol can form hydrogen bonding with both the carbonyl and the hydroxyl groups of the SA molecule, and this competes with the dimerization. Ethyl acetate, acetonitrile and acetone are fairly strong H-bond acceptors and interact with both hydroxyl group hydrogens of SA. For acetonitrile and methanol the same features are also observed in the IR spectra (Figure 3b). Solutions of SA in AA reveal Raman spectra similar to that in chloroform and the SA melt; a strong carbonyl peak appears at 1646 $cm^{-1}$ and a broad shoulder at 1683 $cm^{-1}$. However, it would be inappropriate to suggest SA dimerization in AA because the molar ratio of AA to SA is higher than 20, and it would be difficult to differentiate SA–SA dimerization from SA–AA interactions. A peak at 1615 $cm^{-1}$ in the Raman spectra is mainly due to the ring vibration in SA. This peak is silent in the spectra of the crystalline material, but it is observed in the solution Raman spectra; less clearly in chloroform but more clearly in other solvents.

The spectroscopic findings are summarized in Table 1. With respect to dimerization, the data match previous literature data suggesting the existence of SA as dimerized in chloroform[36] and as monomer in methanol,[37] as well as the findings for benzoic acid that the monomer is favored in ethanol and the dimer in chloroform.[12] In addition to the carbonyl region, the SA dimer formation is also indicated in the bending region of O–H in the Raman spectra. The peak at 1324 $cm^{-1}$ in the solid SA can be assigned to in-plane bending of the carboxyl group.[38] This peak is seen at the same position in the solid SA and in the chloroform solution where SA remains as dimer. However, this peak moves to lower frequency in the solvents where SA exists primarily as monomers.

*Concentration Dependence of the Monomer–Dimer Equilibrium.* Figure 4 shows the SA-chloroform solution spectra at different concentrations. With increase in SA concentration, the peak corresponding to the dimer increases more than the peak corresponding to the monomer suggesting a gradual shift in favor of the dimer formation at increasing SA concentration (10.6 g/kg of SA in chloroform is the highest concentration that could be used at ambient temperature (20–22 °C) without the solution crystallizing).

The concentration effect on the monomer–dimer equilibrium was also examined in the other solvents: ethyl acetate,

**Table 1. Selected Bands in Raman and IR Spectra of SA (in $cm^{-1}$)[a]**

| | Raman spectroscopy | | | IR spectroscopy | |
|---|---|---|---|---|---|
| | ν(C=O) SA monomer | ν(C=O) SA dimer | $\delta$(O–H)$_{carboxyl}$ | ν(C=O) SA monomer | ν(C=O) SA dimer |
| solid SA | | 1637(s) | 1324(s) | | 1655(s) |
| melt SA | 1692(w) | 1641(s) | 1322 | 1686(sh) | 1664(s) |
| chloroform | 1692(w) | 1642(s) | 1324(s) | 1692(sh) | 1664(s) |
| ethyl acetate | 1679(s) | | 1317(s) | | |
| acetonitrile | 1687(s) | | 1316(s) | 1687(s) | |
| acetone | 1672(s) | | 1318(s) | | |
| methanol | 1675(s) | | 1320(s) | 1674(s) | |
| AA | 1683(sh,b) | 1646(s)[b] | 1320(b) | | |

[a]Abbreviations used to describe the peaks: s = strong, sh = shoulder, w = weak, b = broad, v = stretching, $\delta$ = in plane bending. [b]This peak is assumed to primarily reflect interactions related to the AA–SA heterodimer.


dx.doi.org/10.1021/ja503131w | J. Am. Chem. Soc. 2014, 136, 11664–11673

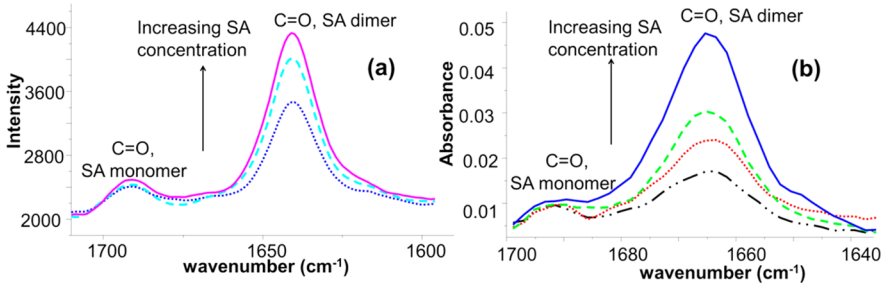


**Figure 4.** (a) Raman spectra of SA in chloroform at different concentrations; 10.63, 9.40, 7.0 g/kg. (b) IR spectra of SA in chloroform at different concentrations; 6.85, 4.56, 3.21, and 2.38 g/kg.

acetonitrile, acetone, and methanol in which SA predominantly exists in monomer form. Unlike SA-chloroform solutions, there was no clear evidence for a shift in equilibrium at increasing SA concentration in methanol (100 and 472 g/kg), acetone (38 and 132 g/kg) and ethyl acetate (97 and 189 g/kg). In acetonitrile, a particularly wide range of relative concentrations (fractions of the solubility) was examined (Figure 4). At 20 °C, the solubility of SA in acetonitrile is 88 g/kg and at concentration as high as 79.075 g/kg, no shift in the carbonyl peak was observed.

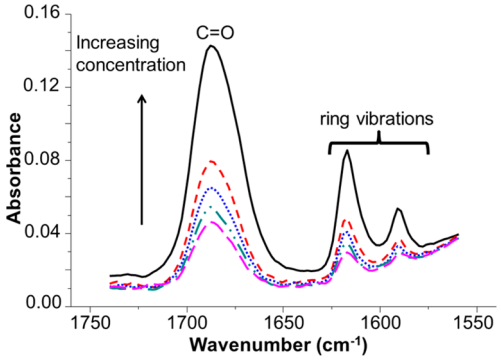


**Figure 5.** IR spectra of SA solutions in acetonitrile at different concentrations; 79.08–20.87 g/kg (79.08, 52.32, 35.80, 26.97, and 20.87 g/kg).

**Solution Calorimetry.** Experimentally determined $\Delta H_{solution}$ for SA in the six different solvents are given in the second column of Table 2. Considering the low concentration in the experiments, these values can be interpreted as essentially being infinite dilution values, $\Delta H^{\infty}_{solution}$.

In addition the table shows the calculated values of enthalpy of solvation, cavity formation and interaction as per eq 1, 3 and 2, respectively. Obviously the enthalpy of solution is a fairly small endothermic difference between the enthalpy of sublimation and the enthalpy of solvation. The enthalpy of solvation, in turn is a large difference between the enthalpy of interaction and the enthalpy of cavity formation, the latter being approximately only half of the former. The table shows that the enthalpy of solvent–solute interaction, $\Delta H_{interaction}$, increases in the order: chloroform, ethyl acetate, acetonitrile acetone, methanol and AA.

**Table 2. Enthalpies of Solution, Solvation, Cavity Formation, and Interaction Per Mole of SA at 25 °C**

| solvents | $\Delta H_{solution}$ (kJ mol$^{-1}$) | $\Delta H_{solvation}$ (kJ mol$^{-1}$) | $\Delta H_{cavity}$ (kJ mol$^{-1}$) | $\Delta H_{interaction}$ (kJ mol$^{-1}$) |
|---|---|---|---|---|
| chloroform | 20.895 ± 0.201 | −73.5 | 51.6 | −123.5 |
| ethyl acetate | 13.062 ± 0.059 | −81.3 | 59.7 | −139.6 |
| acetonitrile | 20.151 ± 0.006 | −74.2 | 66.9 | −139.7 |
| acetone | 12.107 ± 0.008 | −82.2 | 61.0 | −141.9 |
| methanol | 12.173 ± 0.036 | −82.2 | 81.6 | −162.2 |
| AA | 17.173 ± 0.049 | −77.2 | 87.7 | −163.3 |

**DFT Calculations.** *Geometries and Binding Energies of (1:1) Molecular Complexes.* The optimized (1:1) SA-solvent interactions at three distinct sites of the SA molecule: the benzene ring hydrogens (site 1), the benzene ring $\pi$-electrons (site 2), and the carboxyl group (site 3), are shown in Figure 6 for the six solvents. The figure presents equilibrium geometries and binding energies of the molecular complexes for each stable configuration. At site 1, the solvent molecules are bound through weak van der Waals forces to two benzene hydrogens through electronegative atoms (O, N, or Cl). At site 2, an aliphatic part of a solvent molecule locates one of its hydrogens over the center of the benzene ring; an example of binding between carbohydrate hydrogen and benzene $\pi$-electrons. At site 3 the −COOH group acts as both H-bond donor and acceptor, thus facilitating binding with polar species.

The weakest binding of −2.5 kJ mol$^{-1}$ is observed at site 1, when chloroform interacts with benzene hydrogens (Figure 6a). About 3–5 times stronger binding is observed at the site 1 for other solvents, with the strongest value for AA (−12.8 kJ mol$^{-1}$) (Figure 6u). Interestingly, the binding to the benzene ring at site 2 is quite uniform for all the six solvents with an average binding energy of 10.0 ± 0.9 kJ mol$^{-1}$. At site 3 the possible formation of H-bonded heterodimers significantly influences on the binding energy. At this site again the weakest bonding is found for chloroform. Ethyl acetate, acetonitrile, and acetone have reasonably strong H-bond acceptors, and all three have a weak H-bond donating functionality that can support heterodimer formation. The clearly weaker bonding of acetonitrile should be due to the less favorable geometry of the H-bonded heterodimer. Being capable of donating and accepting H-bonds, methanol is expected to bind relatively strongly to the -COOH group of SA molecule at site 3. However, the bonding of −40.9 kJ mol$^{-1}$ (Figure 6s) is not much higher than that of ethyl acetate and acetone, and this is probably due to the unfavorable geometrical conditions in the heterodimer. The strongest binding of −64.5 kJ mol$^{-1}$ has been calculated at site 3 for AA, where the carboxyl group can form two unconstrained H-bonds (Figure 6x).

To complement the solvent–solute interaction, we have also quantified solvent–solvent interactions, and the values given in Figure 6 represent the strongest binary interactions. The most stable solvent associates are dimers, except for in case of methanol (Figure 6t), where a stable tetramer prevails energetically over dimer and trimer. In this case, however,


dx.doi.org/10.1021/ja503131w | J. Am. Chem. Soc. 2014, 136, 11664–11673

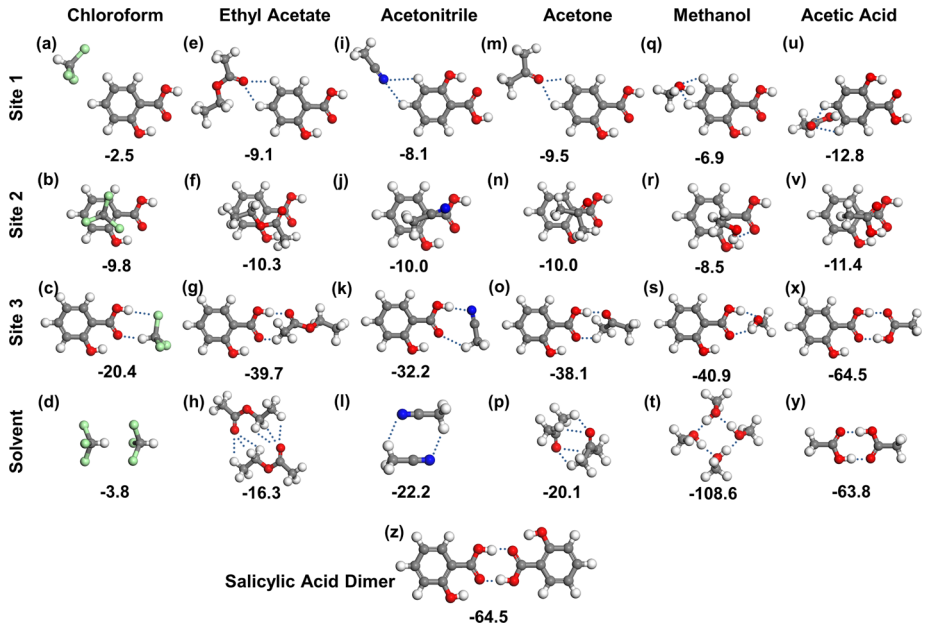


**Figure 6.** Optimized geometries and binding energies (in kJ $mol^{-1}$) for SA-chloroform (1:1) complexes (a–c), chloroform dimer (d), SA-ethyl acetate (e–g), ethyl acetate dimer (h), SA-acetonitrile (i–k), acetonitrile dimer (l), SA-acetone (m–o), acetone dimer (p), SA-methanol (q–s), methanol tetramer (t), SA–AA (u–x), AA dimer (y), and SA dimer, (z) at the B97 D/6-31G(d,p) level. BSSE-corrected binding energies of the molecular complexes are calculated at B2PLYPD/TZVP level. Hydrogen, white; carbon, gray; oxygen, red; nitrogen, blue; chlorine, green.

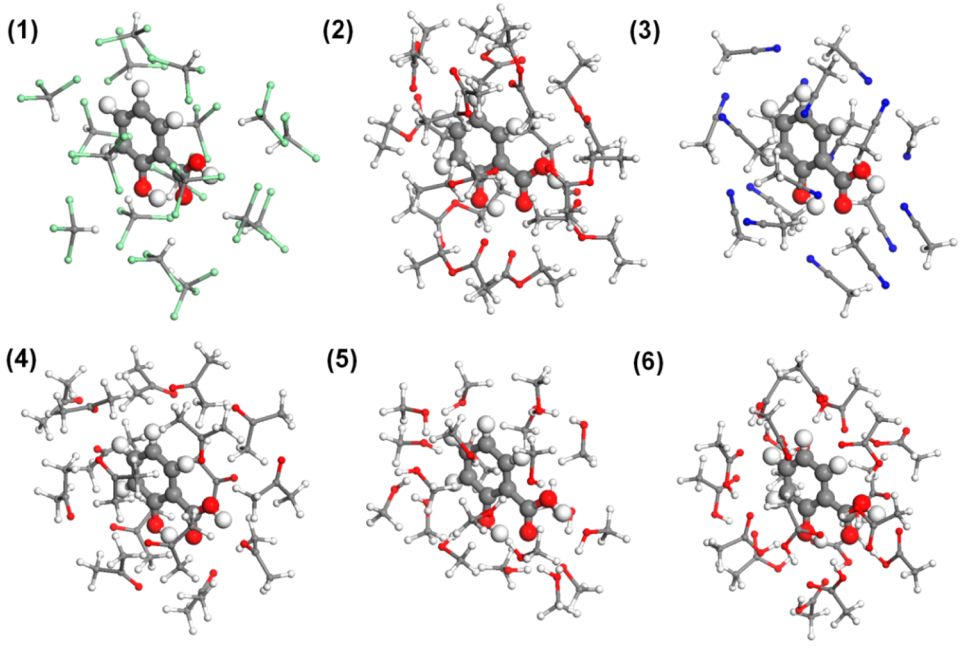


**Figure 7.** Solvation clusters of SA: 17 × chloroform (1), 13 × ethyl acetate (2), 17 × acetonitrile (3), 16 × acetone (4), 20 × methanol (5), and 18 × AA molecule (6); structures fully optimized at the B97D/6-31G(d,p) level. Hydrogen, white; carbon, gray; oxygen, red; nitrogen, blue; chlorine, green.

one can expect that methanol molecules in solution will rather form a network consisting variety of structures. For all solvents the binding between two solvent molecules is more favorable than the solvent-SA bonding at site 1. Except for chloroform where the $CHCl_3\cdots CHCl_3$ solvent pair is stabilized by only −3.8 kJ $mol^{-1}$ (Figure 6d), the binding between two solvent molecules is also stronger than the solvent-SA binding at site 2. On the other hand, all the solvent monomers, except methanol, prefer to bind to the carboxyl group of SA (site 3) giving more stable structures compared to their homodimer counterparts. AA binds to SA giving the most stable structures, regardless of the site of interaction. However, the site 3 AA–SA, the AA dimer, and the SA dimer result in almost the same binding energies of −64.5, −63.8, and −64.5 kJ $mol^{-1}$, respectively (structures x, y, and z, Figure 6). This indicates that in solution the molecules of SA and AA may exist in equilibrium of SA–SA, AA–AA, and SA–AA dimers. In the Supporting Information, a calculated energy profile is presented for transformation of an SA–SA dimer into SA–AA heterodimer, mediated by a molecule of AA. The calculations at B97D/6-


dx.doi.org/10.1021/ja503131w | J. Am. Chem. Soc. 2014, 136, 11664–11673

Table 3. Binding Energies of the Solvation Cluster ($\Delta E_{bind}$) Calculated at B2PLYPD/QZVP Level along With Solvation Shell Densities[a]

| structure | solvation shell-SA | $\Delta E_{bind}$ (kJ mol$^{-1}$) | $\Delta E_{solvation}$ (kJ mol$^{-1}$) | $\Delta E_{deform}$ (kJ mol$^{-1}$) | density (atom/nm$^3$) |
|---|---|---|---|---|---|
| 1 | 17 × chloroform−SA | −156.3 | −69.8 | 0.2 | 57 |
| 2 | 13 × ethyl acetate−SA | −242.0 | −83.8 | 3.6 | 134 |
| 3 | 17 × acetonitrile−SA | −423.6 | −87.2 | 6.4 | 114 |
| 4 | 16 × acetone−SA | −318.1 | −101.3 | 8.3 | 133 |
| 5 | 20 × methanol−SA | −526.1 | −119.8 | 15.8 | 146 |
| 6 | 18 × AA−SA | −637.0 | −184.1 | 23.3 | 125 |

[a]Binding at the interface between the SA molecule and the surrounding solvent molecules is quantified as $\Delta E_{solvation}$. Deformation of SA molecule within a solvation shell is quantified as the energy difference of its solvation-shell (constrained) and fully-relaxed geometry ($\Delta E_{deform}$).

31G(d,p) with the BSSE corrected binding energies at B2PLYPD/TZVP level indicate preferential formation of the SA−AA dimer over the SA−SA dimer. The transition is associated with an activation energy barrier of 4.2 kJ mol$^{-1}$ and a stabilization energy of 2.9 kJ mol$^{-1}$. This supports the view that the vibrational spectra of AA solutions reveal SA−AA heterodimer formation rather than SA−SA dimerization.

*Solvation Cluster Modeling.* The more or less spherical equilibrium geometry of the solvation cluster results from mutual interactions of all molecules forming the cluster and is illustrated in Figure 7. The number of solvent molecules to fill the first solvation shell varies from 13 in case of ethyl acetate having a fairly large molecule to 20 for methanol, being a small molecule forming a dense network of H-bonds (Table 3).

Table 3 reveals that the highest cohesive strength of the solvation cluster, $\Delta E_{bind}$, is found for solvents capable of making strong H-bonds, i.e., AA (−637 kJ mol$^{-1}$) and methanol (−526 kJ mol$^{-1}$). The weakest strength is calculated for chloroform (−156 kJ mol$^{-1}$), consistent with the weakest binding observed for the (1:1) chloroform-chloroform and chloroform-SA dimers. The detailed composition of solvation clusters, relevant solvation shell densities, and binding, solvation, and deformation energies are collated in Table 3.

The calculated solvation energies, $\Delta E_{solvation}$ (Table 3), reveal the bonding to be weakest to the chloroform shell and to increase in the order ethyl acetate, acetonitrile, acetone, methanol, and AA. As further shown in Table 3, the deformation energy of the SA molecule correlates to the strength of binding of the shell to the SA molecule.

## DISCUSSION

The frequency of the carbonyl peak associated with the SA monomer in the Raman spectra (Table 1, column "SA monomer") reflects the strength in the solvent−solute binding at the carbonyl group and should correlate to the DFT calculated (1:1) interaction energy between the solvent molecule and the carboxyl group (site 3) of SA (given in Figure 6). As shown in Figure 8a this correlation is actually quite strong. This corroborates the validity of the DFT computations and shows that the carbonyl peak frequency can be used as a probe for the strength of the solvent−solute interaction.

The DFT computed interaction energy of the solute molecule to the first solvation shell, $\Delta E_{solvation}$, does not account for cavity formation and thermal contributions to the Gibbs free energy at finite temperatures, and for this reason cannot be directly compared to calorimetric enthalpy or Gibbs free energy of solvation. The DFT calculated solvation energy, $\Delta E_{solvation}$, can however be related to the enthalpy of solvent−solute interaction, $\Delta H_{interaction}$, as calculated from experimental

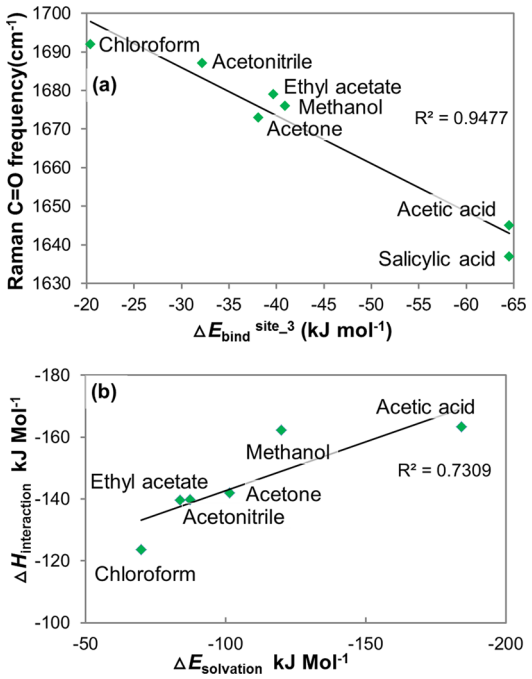


**Figure 8.** Relationship between (a) the carbonyl stretching Raman frequency and the DFT calculated 1:1 interaction energy at the carboxyl site and the (b) enthalpy of interaction, $\Delta H_{interaction}$, obtained from calorimetric data and the DFT calculated solvation energy, $\Delta E_{solvation}$.

calorimetric data using eq 2. As shown in Figure 8b this correlation is reasonably clear, corroborating the validity of the computed solvation energies.

The nucleation experiments,[16] reveal that the difficulty of nucleation and the solid−liquid interfacial energy both increase in the order: chloroform, ethyl acetate, acetonitrile, acetone, methanol, and AA. The crystal structure is based on centrosymmetric dimerization over the carboxyl groups, and the spectroscopic data suggest that in chloroform solution SA exists primarily as SA−SA dimers (Table 1). However, in the other five solvents the spectroscopic data (Table 1) suggests that SA exists primarily in the form of monomers. Accordingly, presence of dimers in the solution does not reveal itself as being a governing factor for the nucleation process.

As shown in Figure 9a, the solid−liquid interfacial energy derived from induction time experiments is reasonably well correlated to the frequency of the carbonyl peak associated with the SA monomer in the Raman spectra (Table 1, column "SA monomer"). As shown in Figure 9b, increasing solid−liquid interfacial energy is also quite clearly correlated to increasing enthalpy of interaction, $\Delta H_{interaction}$, (Table 2).Considering the


dx.doi.org/10.1021/ja503131w | J. Am. Chem. Soc. 2014, 136, 11664−11673

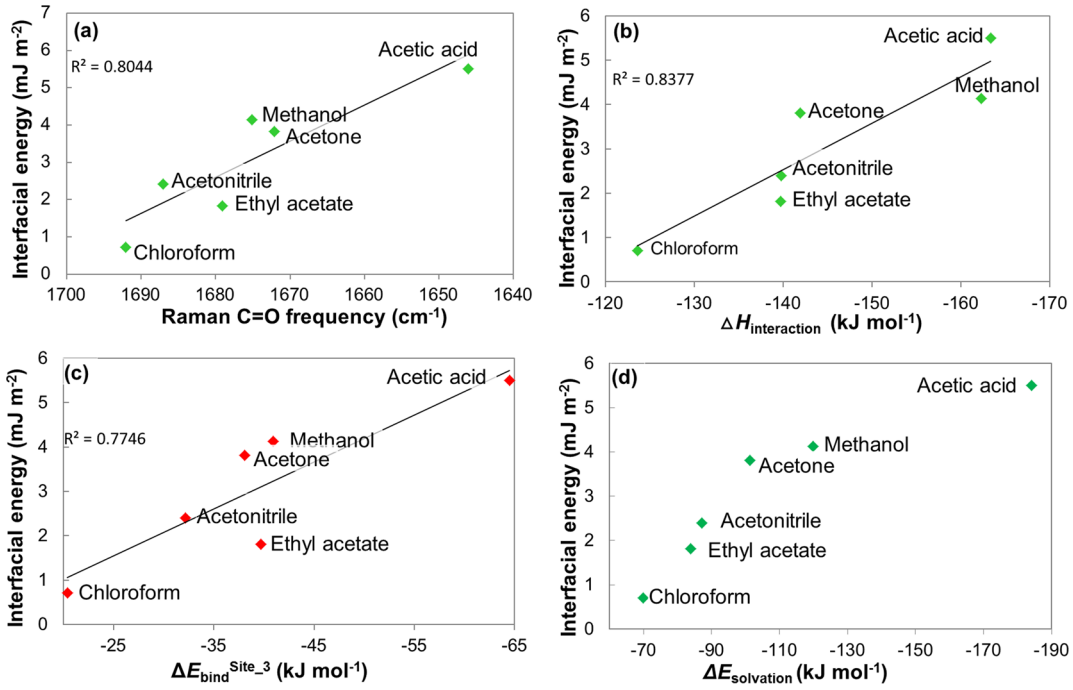


**Figure 9.** Relationship between the difficulty of nucleation as represented by the interfacial energy and (a) carbonyl stretching from Raman spectroscopy (b) enthalpy of interaction, $\Delta H_{interaction}$ derived from calorimetric data and DFT derived (c) 1:1 binding energy at the polar site 3 and (d) solvation energy, $\Delta E_{solvation}$.

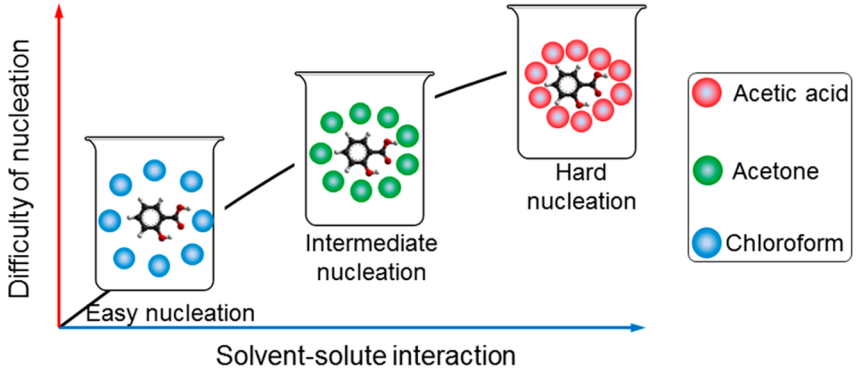


**Figure 10.** Schematic presentation of SA nucleation in solution.

experimental and theoretical uncertainties and approximations of the estimation of the solid–liquid interfacial energy from nucleation experiments using the classical nucleation theory and the solvent–solute interaction enthalpy from calorimetric measurements using eq 2 and the scaled particle theory, this correlation is quite remarkable.

In Figure 9c is shown the solid–liquid interfacial energy derived from the induction time experiments versus the (1:1) binding energy of solvent molecules to the carboxyl group of SA (site 3) calculated by DFT. Obviously, the DFT energy calculation does capture quite well the overall features of the nucleation behavior in the different solvents, even though the behavior in ethyl acetate is not entirely satisfactory. Figure 9d shows that an even better correlation of the solid–liquid interfacial energy is found in the binding energy of the SA molecule to its first solvation shell ($\Delta E_{solvation}$), and now the order of nucleation in the different solvents is captured without exception. It should be noted though that in the nucleation experiments[16] the molar ratio of solvent to solute is chloroform (34), ethyl acetate (4), acetonitrile (16), acetone (3), methanol (4), and AA (9). Compared to the data in Table 3, it can be concluded that a full solvation shell can only be formed around each solute molecule in chloroform. In all the other solvents the concentration of SA is too high for the solvation cluster modeling to be able to give a correct representation of the reality.

Previous experimental results[16] show that AA and, to a slightly lesser extent, methanol and acetone as solvents create molecular environment in which nucleation of SA is difficult, in contrast to the relatively easy nucleation in acetonitrile and ethyl acetate and very easy nucleation in chloroform. The analysis and the discussion above reveal clear relations between the nucleation behavior, spectroscopic observations of molecular interactions in solution, strength of solvent–solute interaction from calorimetric data, and quantum chemical binding energy calculations between solvent molecules and the SA molecule. The binding strength is reasonably well captured by the less demanding DFT computations over the (1:1) bonding at the carboxyl group (site 3) of the SA, suggesting the importance of this binding site. This is not surprising since the


dx.doi.org/10.1021/ja503131w | J. Am. Chem. Soc. 2014, 136, 11664–11673

desolvation of this group is of particular importance for the formation of the SA dimer, on which the crystal structure is based. The binding strength in the solvent−solute interaction is also captured in the calorimetrically determined enthalpy of interaction, $\Delta H_{interaction}$ which matches well with the DFT energy of binding to the first solvation shell, $\Delta E_{solvation}$.

The results support the hypothesis that a stronger binding between the solvent and the solute makes nucleation more difficult. The stronger the solvent binds to the SA molecule in solution, the more stable is the solvent−solute cluster. The desolvation will require more energy and becomes slower, which translates into a more difficult nucleation as is schematically illustrated by Figure 10. The nucleation becomes slower at comparable driving force or a higher driving force is required to reach the same induction time. In accordance with this, in chloroform the dimerization of SA is not regarded to be the prime reason for the ease of nucleation but rather to be understood as another effect of the weak solvent−solute interaction.

## CONCLUSION

Vibration spectroscopy results reveal that in chloroform SA molecules appear primarily as dimers and the dimerization increases with increasing concentration. In ethyl acetate, acetonitrile, acetone and methanol spectroscopic data suggest that SA exists primarily in monomer form with no clear shift towards dimers with increasing concentration. The Raman frequency of the monomer SA carbonyl peak decreases in the order: chloroform, acetonitrile, ethyl acetate, methanol, acetone and AA. The DFT calculated (1:1) interaction energy between a solvent molecule and the carboxyl group of SA increases approximately in the same order, and shows that the carbonyl peak frequency can be used as a probe for the strength of the solvent−solute interaction. The enthalpy of solvent-solute interaction, $\Delta H_{interaction}$, determined from calorimetric measurements in the different solvents increases in the order chloroform, ethyl acetate, acetonitrile, acetone, methanol and AA, and the same order is found in the DFT computed solvation energies, $\Delta E_{solvation}$, i.e. the binding energy of the solvent molecule shell to the solute molecule in the centre. In comparing the results of the present work with previous results on the nucleation of SA in the different solvents, it is found that the order of increasing difficulty of nucleation is clearly correlated to the different measures − spectroscopic, calorimetric and computational − of increasing solvent−solute interaction. The results support the hypothesis that the influence of the solvent on the crystal nucleation is related to the desolvation of the SA molecules. The stronger the solvent binds to the SA molecule in solution, the more difficult the desolvation and the slower the nucleation becomes.

## ASSOCIATED CONTENT

### Supporting Information

Details of cavity calculation, binding energies, SA-AA interactions and additional IR and Raman data. This material is available free of charge via the Internet at http://pubs.acs.org.

## AUTHOR INFORMATION


### Corresponding Author

rasmuson@ket.kth.se


### Notes

The authors declare no competing financial interest.

## ACKNOWLEDGMENTS

The support of the Science Foundation Ireland (10/IN.1/B3038) is gratefully acknowledged. Å.R. gratefully acknowledges the support of the Swedish Research Council (621-2010-5391). J.Z. acknowledges the Science Foundation Ireland (SFI) and Higher Education Authority funded Irish Centre for High End Computing (ICHEC) for access to computational facilities.

## REFERENCES


(1) Erdemir, D.; Lee, A. Y.; Myerson, A. S. *Acc. Chem. Res.* **2009**, *42*, 621.
(2) Davey, R. J.; Schroeder, S. L.; ter Horst, J. H. *Angew. Chem., Int. Ed. Engl.* **2013**, *52*, 2166.
(3) Vekilov, P. G. *Cryst. Growth Des.* **2010**, *10*, 5007.
(4) Granberg, R. A.; Ducreux, C.; Gracin, S.; Rasmuson, Å. C. *Chem. Eng. Sci.* **2001**, *56*, 2305.
(5) Teychene, S.; Biscans, B. *Cryst. Growth Des.* **2008**, *8*, 1133.
(6) Svärd, M.; Rasmuson, Å. C. *Cryst. Growth Des.* **2013**, *13*, 1140.
(7) Zahn, D.; Anwar, J. *Chem.−Eur. J.* **2011**, *17*, 11186.
(8) Janik, M.; Malarski, Z.; Mrozinski, J.; Wajcht, J.; Zborucki, Z. *J. Crystallogr. Spectrosc. Res.* **1991**, *21*, 519.
(9) Svärd, M.; Nordström, F. L.; Jasnobulka, T.; Rasmuson, Å. C. *Cryst. Growth Des.* **2010**, *10*, 195.
(10) Etter, M. C. *Acc. Chem. Res.* **1990**, *23*, 120.
(11) Kulkani, S. A.; McGarrity, E. S.; Meekes, H.; ter Horst, J. H. *Chem. Commun.* **2012**, *48*, 4983.
(12) Davey, R. J.; Dent, G.; Mughal, R. K.; Parveen, S. *Cryst. Growth Des.* **2006**, *6*, 1788.
(13) Anwar, J.; Zahn, D. *Angew. Chem., Int. Ed.* **2011**, *50*, 1996.
(14) Wallace, A. F.; Hedges, L. O.; Fernandez-Martinez, A.; Raiteri, P.; Gale, J. D.; Waychunas, G. A.; Whitelam, S.; Banfield, J. F.; De Yoreo, J. J. *Science* **2013**, *341*, 885.
(15) Moon, C.; Taylor, P. C.; Rodger, P. M. *J. Am. Chem. Soc.* **2003**, *125*, 4706.
(16) Mealey, D.; Rasmuson, Å. C. *Cryst. Eng. Comm.*; submitted.
(17) Acree, W.; Chickos, J. S. *J. Phys. Chem. Ref. Data* **2010**, *39*, 043101.
(18) Bennaim, A.; Marcus, Y. *J. Chem. Phys.* **1984**, *81*, 2016.
(19) Jesus, A. J. L.; Tome, L. I. N.; Eusebio, M. E. S.; Redinha, J. S. *J. Phys. Chem. B* **2006**, *110*, 9280.
(20) Solomonov, B. N.; Novikov, V. B. *J. Phys. Org. Chem.* **2008**, *21*, 2.
(21) Reiss, H.; Frisch, H. L.; Lebowitz, J. L. *J. Chem. Phys.* **1959**, *31*, 369.
(22) Pierotti, R. A. *Chem. Rev.* **1976**, *76*, 717.
(23) Costa, F. S.; Eusebio, M. E.; Redinha, J. S.; Leitao, M. L. P. *J. Chem. Thermodyn.* **2000**, *32*, 311.
(24) Barannikov, V. P.; Guseynov, S. S.; Vyugin, A. I. *J. Chem. Thermodyn.* **2004**, *36*, 277.
(25) Salamanca, Y. P.; Blanco, L. H.; Vargas, E. F. *J. Therm. Anal. Calorim.* **2013**, *114*, 451.
(26) Moreldesrosiers, N.; Morel, J. P. *Can. J. Chem.* **1981**, *59*, 1.
(27) Tang, K. E. S.; Bloomfield, V. A. *Biophys. J.* **2000**, *79*, 2222.
(28) Frisch, M. J.; Trucks, G. W.; Schlegel, H. B.; Scuseria, G. E.; Robb, M. A.; Cheeseman, J. R.; Scalmani, G.; Barone, V.; Mennucci, B.; Petersson, G. A.; Nakatsuji, H.; Caricato, M.; Li, X.; Hratchian, H. P.; Izmaylov, A. F.; Bloino, J.; Zheng, G.; Sonnenberg, J. L.; Hada, M.; Ehara, M.; Toyota, K.; Fukuda, R.; Hasegawa, J.; Ishida, M.; Nakajima, T.; Honda, Y.; Kitao, O.; Nakai, H.; Vreven, T.; Montgomery, J. A., Jr.; Peralta, J. E.; Ogliaro, F.; Bearpark, M.; Heyd, J. J.; Brothers, E.; Kudin, K. N.; Staroverov, V. N.; Kobayashi, R.; Normand, J.; Raghavachari, K.; Rendell, A.; Burant, J. C.; Iyengar, S. S.; Tomasi, J.; Cossi, M.; Rega, N.; Millam, N. J.; Klene, M.; Knox, J. E.; Cross, J. B.; Bakken, V.; Adamo, C.; Jaramillo, J.; Gomperts, R.; Stratmann, R. E.; Yazyev, O.; Austin, A. J.; Cammi, R.; Pomelli, C.; Ochterski, J. W.; Martin, R. L.; Morokuma, K.; Zakrzewski, V. G.; Voth, G. A.; Salvador, P.; Dannenberg, J. J.; Dapprich, S.; Daniels, A. D.; Farkas, Ö.; Foresman,

J. B.; Ortiz, J. V.; Cioslowski, J.; Fox, D. J. *Gaussian 09*, rev. b01; Gaussian, Inc.: Wallingford CT, 2009.
(29) Grimme, S. *J. Comput. Chem.* **2006**, *27*, 1787.
(30) Muller-Dethlefs, K.; Hobza, P. *Chem. Rev.* **2000**, *100*, 143.
(31) Schwabe, T.; Grimme, S. *Phys. Chem. Chem. Phys.* **2007**, *9*, 3397.
(32) Rassolov, V. A.; Ratner, M. A.; Pople, J. A.; Redfern, P. C.; Curtiss, L. A. *J. Comput. Chem.* **2001**, *22*, 976.
(33) Schaefer, A.; Huber, C.; Ahlrichs, R. *J. Chem. Phys.* **1994**, *100*, 5829.
(34) Boys, S. F.; Bernardi, F. *Mol. Phys.* **1970**, *19*, 553.
(35) Weigend, F.; Ahlrichs, R. *Phys. Chem. Chem. Phys.* **2005**, *7*, 3297.
(36) Dunn, G. E.; McDonald, R. S. *Can. J. Chem.* **1969**, *47*, 4577.
(37) Ke, J.; Jin, S. Z.; Han, B. X.; Yan, H. K.; Shen, D. Y. *J. Supercrit. Fluids* **1997**, *11*, 53.
(38) Elbagerma, M. A.; Edwards, H. G. M.; Munshi, T.; Hargreaves, M. D.; Matousek, P.; Scowen, I. J. *Cryst. Growth Des.* **2010**, *10*, 2360.